



Surface tuning of noble metal doped perovskite oxide by synergistic effect of thermal treatment and acid etching: A new path to high-performance catalysts for methane combustion

Xinwei Yang¹, Qin Gao¹, Zhenyang Zhao, Yanglong Guo, Yun Guo, Li Wang, Yunsong Wang, Wangcheng Zhan*

Key Laboratory for Advanced Materials and Research Institute of Industrial Catalysis, School of Chemistry and Molecular Engineering, East China University of Science and Technology, Shanghai, 200237, PR China



ARTICLE INFO

Keywords:

Perovskite oxide
Noble metal
Thermal treatment
Acid etching
Surface structure

ABSTRACT

Perovskite oxides containing noble metals have been widely used as heterogeneous catalysts for a broad range of important chemical reactions in recent decades, especially in environmental catalysis. However, it is still a great challenge to develop a facile strategy for tuning the distribution of noble metal on the perovskite oxide to prepare a perovskite catalyst with unexpected catalytic performance. Herein, we proposed a new path to tune the distribution of noble metal on the perovskite oxide by synergistic effect of thermal treatment and acid etching. After calcining at high temperatures (800/900 °C vs 500/700 °C), those Pd species on the LaAl_{0.9}Pd_{0.1}O₃ catalyst would gradually exsolve from the bulk phase to the surface and subsurface of the catalyst, which was confirmed by X-ray diffraction (XRD), Raman spectra, X-ray photoelectron spectroscopy (XPS), high resolution transmission electron microscopy (HRTEM) and CO-pulse experiment. These *in situ*-generated Pd species on the surface and subsurface of the catalyst can significantly improve the redox property of the LaAl_{0.9}Pd_{0.1}O₃ catalyst. As a result, unexpected low-temperature catalytic activity and remarkable high stability for CH₄ combustion were achieved on the LaAl_{0.9}Pd_{0.1}O₃ catalyst. On this basis, the surface composition of the LaAl_{0.9}Pd_{0.1}O₃ catalyst was further modulated by HNO₃ etching. Part of the La element can be selectively etched away from the LaAl_{0.9}Pd_{0.1}O₃ framework, and more Pd-site terminated perovskite surfaces are created after acid treatment, leading to the further promotion of catalytic activity of the LaAl_{0.9}Pd_{0.1}O₃ catalyst for CH₄ combustion.

1. Introduction

Natural gas has been widely used in power generation and other heating applications through the process of combustion due to its large quantities throughout the world and high calorific value. However, the incomplete combustion of natural gas would lead atmospheric pollution since methane (the main component of natural gas) has a greenhouse effect greater than twenty times that of CO₂. Moreover, the direct combustion of natural gas would result in the formation of toxic nitrogen oxides (NO_x) due to the condition of high temperature. The catalytic combustion is a promising method to increase the combustion efficiency and effectively lower the combustion temperature to decrease the emission of the noxious hydrocarbon and NO_x [1–3].

Methane (CH₄) has a very stable and highly symmetrical structure, which causes a huge challenge for the catalyst to activate CH₄ at low

temperature and decrease the ignition temperature. Meanwhile, the ideal catalysts is able to preserve excellent performance under varied operating conditions, such as relatively high space velocity and reactant gas humidity. Besides, the catalyst is required to have good thermal stability, because catalytic combustion of CH₄ is usually operated out at high temperature. There is a general consensus that Pd-based catalysts are the most active catalysts for methane combustion [4,5]. Its catalytic performances are dependent on the state of Pd species, support property and the interaction between Pd and the support so on [6–8]. In spite of extensive studies, Pd-based catalyst with an excellent ignition activity and high thermal stability is still desired for methane combustion. For example, the PdO_x nanoparticles, regarded as the main active phase, are inclined to agglomerate during the reaction at high temperature, and even decompose at temperatures higher than 650 °C, leading to catalyst deactivation [9,10]. Besides, the poor thermal stability of the

* Corresponding author.

E-mail address: zhanwc@ecust.edu.cn (W. Zhan).

¹ These two authors contributed equally to this paper.

support is also the main cause of supported Pd catalyst deactivation [11–13].

Perovskites oxides characterized by an ABO_3 structure have been widely studied as heterogeneous catalysts for a broad range of important chemical reactions in recent decades, especially in environmental catalysis, because of their flexible composition, excellent redox properties, and superior thermal and hydrothermal stabilities [14–21]. However, perovskite oxides usually exhibit unsatisfactory catalytic performances in oxidation reactions, due to the following reason [22,23]. The native perovskite surface is preferentially A-site, not catalytic active sites, terminated to the detriment of the B sites [24–26]. In addition, calcination at high temperature during the preparation process is essential to the construction of the perovskite structure, which would result in an ultra-low surface area of perovskites oxide. Therefore, in order to make full use of the advantages of perovskites oxides, it is urgent to enhance the catalytic performance of perovskites oxides.

Up to now, one of the most effective strategies was the substitution of A or B cations in perovskite oxides with other metal elements [27–32]. Through the fabrication of more structural defects on the surface of perovskites oxides, their catalytic performances can be markedly improved [33–35]. Compared to A-site substitution in perovskites oxide, B-site substitution is typically more effective in improving the catalytic performances of perovskite oxides because B-site cations play the role of the catalytic performance of perovskite oxides. On this basis, B-site substitution with a noble metal is better than with a transition metal, since noble metals usually possess super high catalytic performances for a large number of reactions [36–38]. The more gratifying part is that construction of the noble metal in the matrix of perovskite oxide can also significantly improve the thermal stability of the noble metal species at high temperature [39]. However, the incorporation of noble metal into the perovskite would reduce the utilization of noble metal, because most of the noble metal in the B sites of the perovskite lattice cannot participate in the catalytic reaction occurring on the catalyst surface. Therefore, as mentioned above, B-site substitution with noble metal is not enough to acquire perovskite oxide with truly efficient catalytic performances. It is still necessary to explore a new and simple method to modulate the surface structure and composition of those noble metal doped perovskites, in order to expose the noble metal incorporated into the B site of the perovskite lattice as close as possible to the surface and subsurface of perovskite oxide.

Fortunately, many literature investigations have reported the migration of noble metal incorporated into the B site of the perovskite lattice [24]. For example, when the perovskite catalyst substituted with a noble metal is cycled between oxidative and reductive atmospheres, noble metal incorporated into the B site reversibly moved into and out of the perovskite lattice [40–42]. Furthermore, based on first-principles calculations, it was reported that Pd species would segregate in the vicinity of the surface in the form of $LaPdO_{3-y}$ when the perovskite catalyst substituted with Pd was calcined at 800 °C or higher temperatures [43,44]. These results revealed that it is possible to tune the position of noble metal incorporated into the B site of the perovskite lattice by thermal treatment under certain conditions. As a result, the contact between the reactant and noble metal species can be enhanced, leading to the improvement in the catalytic performances of noble metal-doped perovskite oxide. On the other hand, another method of modulating the perovskite surface to expose the noble metal in the B sites of the perovskite lattice to the surface of perovskite oxide was developed through acid/base treatment of perovskite oxides recently [45–48]. Part of the A element can be selectively etched away from the ABO_3 framework of perovskite oxide and more B-site terminated perovskite surfaces are created after acid/base treatment [49]. To summarize, the problem of the low utilization of noble metals incorporated into the B site of the perovskite lattice can be solved by thermal treatment and acid/base treatment in principle. However, to the best of our knowledge, there is no experimental reported on this strategy to synthesize noble metal doped perovskite oxide with excellent catalytic

performance at the present.

Herein, $LaAl_{0.9}Pd_{0.1}O_3$ perovskite catalyst was prepared by the citric acid sol-gel method and calcined at different temperatures. Based on various characterizations, the evolution of the structure of the perovskite catalyst originating from different calcination temperatures, especially the migration of Pd species, was evaluated. Furthermore, the physicochemical properties and catalytic performance of $LaAl_{0.9}Pd_{0.1}O_3$ perovskite catalyst for methane combustion were detected. The results revealed that Pd species in the $LaAl_{0.9}Pd_{0.1}O_3$ catalyst can be reliably exposed to the surface and subsurface of perovskite oxide after calcination at high temperature, which can significantly improve its redox property and catalytic activity for CH_4 combustion. On this basis, the surface composition of the $LaAl_{0.9}Pd_{0.1}O_3$ catalyst calcined at high temperature was further modulated by HNO_3 etching. As a result, more Pd species were generated on the surface of the $LaAl_{0.9}Pd_{0.1}O_3$ catalyst, leading to further enhancement of its catalytic activity for CH_4 combustion. Through the research above, we aim to provide a new strategy to synthesize noble metal doped perovskite catalyst with excellent catalytic performance and excellent thermal stability for CH_4 combustion, which is of great significance to promote the application of perovskite catalyst.

2. Experimental section

2.1. Catalyst preparation

The $LaAl_{0.9}Pd_{0.1}O_3$ catalyst was synthesized by the citric acid sol-gel method. 0.01 mol of $La(NO_3)_3 \cdot 6H_2O$, 0.009 mol of $Al(NO_3)_3 \cdot 9H_2O$, 0.001 mol of $Pd(NO_3)_2$ and citric acid ($C_6H_8O_7$) were dissolved in 30 mL of deionized water. The molar ratio of citric acid to metal ion was 1:1. Then, the solution was evaporated at 80 °C under continued stirring until a gel was formed. The obtained sample was dried at 110 °C for 12 h, and then calcined at 500, 700, 800 and 900 °C for 3 h, respectively. The obtained samples were labelled as LAP-500, LAP-700, LAP-800 and LAP-900.

A $LaAlO_3$ sample with a La:Al molar ratio of 1:1 was also prepared with the same procedures as the $LaAl_{0.9}Pd_{0.1}O_3$ catalyst except for the addition of $Pd(NO_3)_2$. The obtained sample was calcined at 900 °C for 3 h and denoted as LA-900.

After the preparation of the LAP-900 sample, it was treated with concentrated nitric acid for 30 and 90 min, respectively, and then the sample was washed with deionized water three times and dried at 80 °C for 12 h. The obtained samples were denoted as LAP-H-30 and LAP-H-90.

2.2. Catalysts characterization

The powder X-ray diffraction (XRD) patterns were collected on a Bruker D8 Focus diffractometer with $Cu K\alpha$ radiation ($\lambda = 1.54056 \text{ \AA}$) operated at 40 kV and 40 mA. TEM images were obtained on a JEOL 2100 F electron microscope operated at 200 kV. The sample measured was first dispersed in ethanol and then collected on copper grids covered with carbon film. Raman spectra were recorded on a Renishaw Raman ion. X-ray photoelectron spectroscopy (XPS) spectra were obtained at 25 °C on a PHI-Quantera spectrometer under ambient conditions, and the 514 nm line of a Spectra Physics Ar^+ laser was used for excitat SXM spectrometer with $Al K\alpha$ (1486.6 eV) radiation as the excitation source under ultra-high vacuum ($6.7 \times 10^{-8} \text{ Pa}$). All binding energies (BE) were determined with respect to the C1s line (284.8 eV) originating from adventitious carbon.

The temperature-programmed reduction of H_2 (H_2 -TPR) was carried out on a TPDRO 1100 (CE Instruments) with a thermal conductivity detector (TCD). 50 mg of catalyst was filled into the reactor and then directly heated from room temperature to 800 °C at a rate of 10 °C/min in a flow of 5 vol. % H_2/N_2 (50 mL/min).

The temperature-programmed desorption of O_2 (O_2 -TPD) was

conducted using a Micromeritics AutoChem II 2920 equipment associated with a computer-interfaced quadrupole mass spectrometer (Hiden HPR 20). 50 mg of catalyst was pre-treated with 20 vol.% O₂/N₂ (50 mL/min) at 500 °C for 40 min, then cooled to room temperature and kept in 20 vol.% O₂/N₂ (50 mL/min) for 1 h. After being purged with He for 1 h, the sample was heated from 30 to 800 °C at a rate of 10 °C/min in a flow of He (40 mL/min). The signal of O₂ desorbed from the samples was measured by the quadrupole mass spectrometer.

CO pulse experiment was also conducted using the Micromeritics AutoChem II 2920 equipment associated with a computer-interfaced quadrupole mass spectrometer (Hiden HPR 20). The sample was first reduced with 5 vol. % H₂/N₂ (40 mL/min) at 200 °C for 1 h and then cooled to room temperature in a flow of He (40 mL/min). Several pulses of CO were introduced into the sample until no more adsorption was observed.

2.3. Catalytic activity testing

The catalytic performance of the samples prepared for CH₄ combustion was tested in a fixed bed quartz reactor. 200 mg of catalyst (40–60 mesh) was used in the test. The feed gas consisted of 1 vol.% CH₄, 20 vol.% O₂ and N₂ balance with a flow rate of 50 mL/min. The temperature of the catalyst bed was programmed from 150 to 800 °C at a rate of 4 °C/min. The conversion of CH₄ was measured after the catalytic reaction by an online gas chromatograph (Agilent GC 7890 A). The CH₄ conversion (X_{CH₄}) was calculated using the following equation:

$$X = \frac{[CH_4]_{in} - [CH_4]_{out}}{[CH_4]_{in}} \times 100\%$$

where [CH₄]_{in} and [CH₄]_{out} are the CH₄ concentrations in the inlet and outlet gas, respectively.

2.4. Reaction kinetics measurement

The kinetic parameters for CH₄ oxidation were measured at 450 °C in a fixed-bed reactor operated in a differential mode with CH₄ conversion below 15%. The catalytic reaction data were obtained after 30 min of stable reaction. Turnover frequency (TOF) (s⁻¹) was calculated with TOF = X_{CH₄} V_{CH₄} N_A / N, where X_{CH₄} is the conversion of CH₄, V_{CH₄} is the gas flow rate (mol/s) of CH₄, N_A is Avogadro constant and N is the number of catalytically active sites (N = N_{total} · D_{Pd}). The Pd dispersion (D_{Pd}) was measured by CO chemical adsorption at 30 °C (CO/Pd = 1/1) on a micromeritics AutoChem II 2920 chemical adsorption instrument. N_{total} is total atom numbers of Pd, which can be calculated with N_{total} = (m_{Pd} / M_{Pd}) × N_A, where m_{Pd} is the mass of Pd and M_{Pd} is relative atomic mass of Pd.

3. Results and discussion

3.1. Structural characterization of the catalyst

3.1.1. XRD

Fig. 1 showed XRD patterns of the LaAl_{0.9}Pd_{0.1}O₃ catalysts calcined at different temperatures and after HNO₃ etching. Noticeably, the LAP-500 and LAP-700 catalysts hardly exhibited any diffraction peaks, indicating the amorphous phase for these two catalysts. However, when the calcination temperature was increased to 800 and 900 °C, the LAP-800 and LAP-900 catalysts exhibited the characteristic diffraction peaks of perovskite structure (JCPDS 31-0022). Additionally, there was no other diffraction peak of Pd species (metallic Pd or PdO), indicating that all Pd species were highly distributed on the LAP-800 and LAP-900 catalysts. On the other hand, as shown in Fig. 1B, the diffraction peaks of the LAP-900 catalyst shifted slightly to a lower 2θ value compared to the LAP-900 catalyst. Accordingly, the lattice parameter for the LAP-900 catalyst (a = 5.3577 Å, c = 13.0981 Å) was higher than that of the LAP-900 catalyst (a = 5.3506 Å, c = 13.0368 Å) (as shown in Table 1).

Because the cation radius of Pd (+1, 59 pm; +2, 86 pm) is larger than that of Al³⁺ (53.5 pm), when Pd was incorporated into the B site of the perovskite lattice, its lattice parameter will increase, which confirmed that Pd cations have been successfully incorporated into the perovskite lattice [36–38]. After the HNO₃ etching, the LAP-H-30 and LAP-H-90 catalysts still maintained the perovskite structure, but the intensity of the corresponding diffraction peaks decreased compared to the LAP-900 catalyst, indicating the decrease in the crystallite degree of the LAP-900 catalyst after the HNO₃ treatment. Additionally, four new diffraction peaks at 33, 42, 56 and 72° appeared for the LAP-H-90 catalyst and were assigned to the PdO particles (JCPDS 41-1107), indicating that a certain amount of agglomerated PdO species was present on the surface of the LAP-H-90 catalyst. On the other hand, as shown in Fig. 1B, the diffraction peaks for the LAP-H-30 and LAP-H-90 catalysts slightly shifted to the higher 2θ value compared to the LAP-900 catalyst. Accordingly, the lattice parameter for the LAP-H-30 and LAP-H-90 catalysts was lower than that of the LAP-900 catalyst (as shown in Table 1). These results demonstrated that lattice shrinkage occurred after the acid etching of the LAP-900 catalyst, consistent with previous works [50–53].

3.1.2. Raman spectra

Raman spectroscopy is widely used to investigate the surface structure of catalysts. Here, Raman spectroscopy was also applied to investigate the state of the Pd species on the perovskite catalysts calcined at different temperatures. As shown in Fig. 2, for the LAP-500 and LAP-700 catalysts, only Raman peaks with a very low intensity were observed due to the amorphous phase of the catalysts. Moreover, Raman peaks related to the Pd species were absent, demonstrating that all Pd species were highly distributed in the bulk phase. In contrast, the LAP-800 and LAP-900 catalysts exhibited completely different Raman spectra from that of the LAP-500 and LAP-700 catalysts. There were four peaks centred at 273, 439, 646 and 669 cm⁻¹ for the LAP-800 and LAP-900 catalysts. It was reported that the peak at approximately 650 cm⁻¹ can be attributed to the vibration of Pd–O bond in Eg mode [54,55]. Therefore, the peaks at 646 and 669 cm⁻¹ in Fig. 2 can be assigned to the vibration of Pd–O bond under different circumstances, i.e., PdO species on the surface and subsurface of the catalyst, respectively. Compared to the LAP-500 and LAP-700 catalysts, the appearance of these peaks for the LAP-800 and LAP-900 catalysts demonstrated the existence of more PdO species on the surface and subsurface of these two catalysts, indicating that the calcination of the catalyst at high temperature can promote the exposure of Pd species from the bulk phase to the surface and subsurface of the catalysts. Furthermore, as shown in Fig. 2, compared to the LAP-800 catalyst, the ratio of the 646 cm⁻¹ peak intensity to 669 cm⁻¹ peak intensity was increased for the LAP-900 catalyst, indicating more Pd–O bond on the surface and less on the subsurface of the LAP-900 catalyst. This change further confirmed the migration of Pd species to the perovskite surface after the calcination of the LaAl_{0.9}Pd_{0.1}O₃ catalysts at high temperature.

3.1.3. TEM and SEM

To visually investigate the state of Pd species on the LAP-800 and LAP-900 catalysts, TEM and HR-TEM images were obtained and the results are shown in Figs. S1–S2 and Fig. 3. It was obvious that PdO_x particles with a size of about 5–9 nm can be found on the subsurface of the LAP-800 catalyst, while PdO_x particles with a size of about 4–7 nm can be found on both the surface and the subsurface of the LAP-900 catalyst. In HR-TEM image of the LAP-900 catalyst, the interplanar lattice spacing of 2.67 Å corresponded to the (002) crystal plane of PdO. These results further proved the presence of PdO species on the surface and subsurface of the LAP-900 catalyst, originating from the migration of the Pd species during the calcination of the LaAl_{0.9}Pd_{0.1}O₃ catalysts at high temperature, which was consistent with the results of XRD and Raman spectra.

To evaluate the effect of HNO₃ etching on the morphology of the

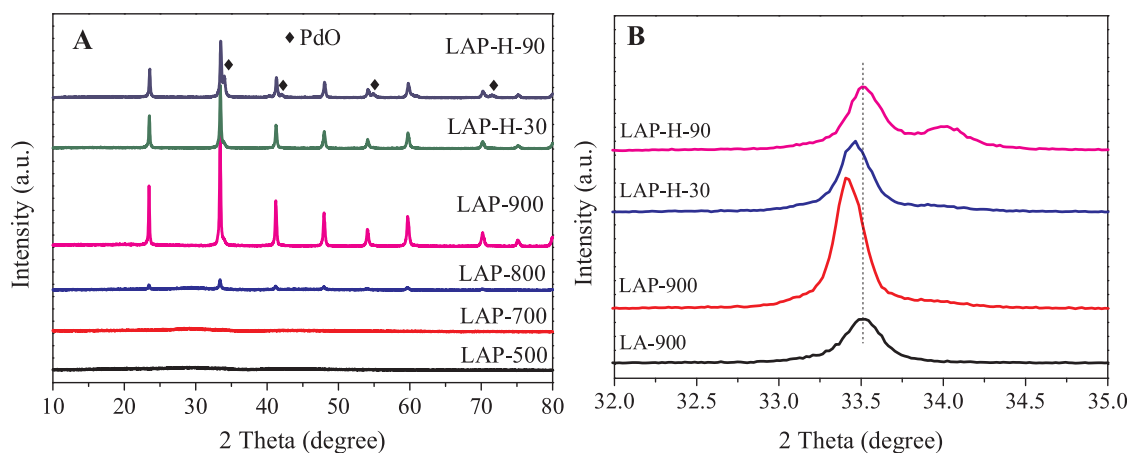


Fig. 1. XRD patterns of the catalysts (A), and the local enlarged patterns of the LA-900, LAP-900, LAP-H-30 and LAP-H-90 catalysts (B).

LAP-900 catalyst, SEM images of the LAP-900-H-30 and LAP-H-90 catalysts were obtained. As shown in Fig. 3D, E and F, the LAP-900 catalyst showed a dense and smooth surface, and there were less holes on the surface. This was in good accordance with its relatively low surface area ($13.5 \text{ m}^2/\text{g}$) (Table 1). However, after HNO_3 etching, the smooth surface of the LAP-900 catalyst was completely destructed and the surface of the LAP-H-30 and LAP-H-90 catalysts looked like a sponge with a large number of holes. Consequently, the surface areas of the LAP-H-30 and LAP-H-90 catalysts significantly increased to 17.4 and $40.7 \text{ m}^2/\text{g}$, respectively. On the other hand, TEM images of the LAP-H-90 catalyst (Fig. S3) showed that the PdO particle with large size (about 20–30 nm) appeared on the surface of the LAP-H-90 catalyst, which was consistent with XRD result.

3.1.4. CO-pulse

It is well known that CO-pulse experiment is usually applied to detect the metal dispersion of supported catalysts. Therefore, CO-pulse experiment can be carried out to evaluate the exposed Pd species on the surface of the LAP catalysts, and then confirm the migration of Pd species based on the calcination of the $\text{LaAl}_{0.9}\text{Pd}_{0.1}\text{O}_3$ catalysts at high temperature. As shown in Fig. S4, the intensity of CO signal ($m/z = 28$) during the first two pulses on the LAP-900 catalyst was much lower than that on the LAP-500 catalyst. As the catalyst was first reduced by H_2 (details shown in Experimental Section), the decrease in the intensity of CO signal was attributed to the chemisorption of CO on Pd atoms exposed on the surface of catalyst. Therefore, the larger amount of CO uptake in the CO-pulse experiment for the LAP-900 catalyst revealed that more Pd atoms migrated from the bulk phase and exposed on the surface in comparison to the LAP-500 catalyst.

Table 1

Surface area, Pd content, lattice parameter, surface composition, Pd dispersion and TOFs (450°C) for all the catalysts.

Samples	Surface area (m^2/g)	Pd content (%) ^a	Lattice parameter (\AA)	Surface composition (atomic ratio) ^b			Pd dispersion (%)	TOF $\cdot 10^2$ (s^{-1}) ^c
				La/La + Al + Pd	Al/La + Al + Pd	Pd/La + Al + Pd		
LA-900	12.0	/	$a = 5.3506, c = 13.0368$	41.9%	58.1%	0%	/	/
LAP-500	12.3	4.9	/	38.3%	59.8%	1.9%	4.30	0.71
LAP-700	12.0	4.9	/	38.7%	59.3%	2.0%	4.89	1.55
LAP-800	11.3	4.7	$a = 5.3651, c = 12.7116$	39.1%	58.7%	2.2%	4.95	2.82
LAP-900	13.5	4.2	$a = 5.3577, c = 13.0981$	39.2%	58.5%	2.3%	8.76	4.66
LAP-H-30	17.4	4.7	$a = 5.3418, c = 13.0800$	34.3%	56.2%	9.5%	8.70	9.63
LAP-H-90	40.7	8.9	$a = 5.3272, c = 13.0323$	28.3%	42.8%	28.9%	5.61	11.83

^a Measured by ICP.

^b Calculated by the XPS data.

^c Tested at 450°C .

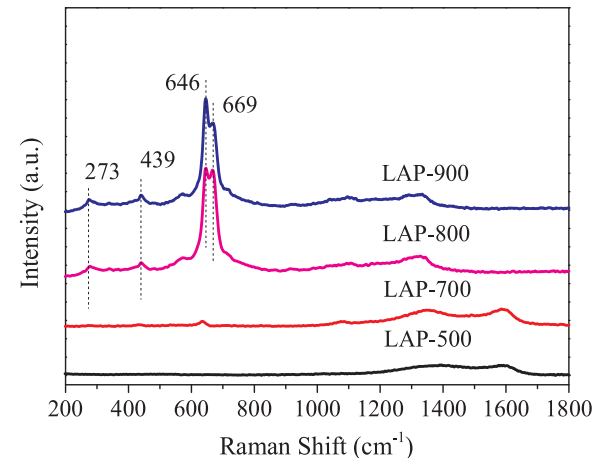


Fig. 2. Raman spectra of the LAP-500, LAP-700, LAP-800 and LAP-900 catalysts.

3.1.5. XPS

Fig. 4 showed Pd 3d XPS spectra of the different catalysts. The Pd 3d_{5/2} binding energies for the LAP-500, LAP-700, LAP-800 and LAP-900 catalysts were 337.8, 337.1, 336.9 and 337.0 eV, respectively. As reported previously, the binding energy of Pd° is 335.1–335.4 eV, and 336.1–336.5 eV for Pd^{2+} and 337.7–338.2 eV for Pd^{4+} [56]. Therefore, Pd species for all of the catalysts prepared were in the form of Pd^{8+} ($\delta > 2$), indicating the strong interaction between the Pd species and perovskite matrix [57–59]. With the increased calcination temperature of the catalyst from 500 to 800°C , the Pd 3d_{5/2} XPS peak slightly shifted to a lower binding energy, indicating the weakening of the interaction

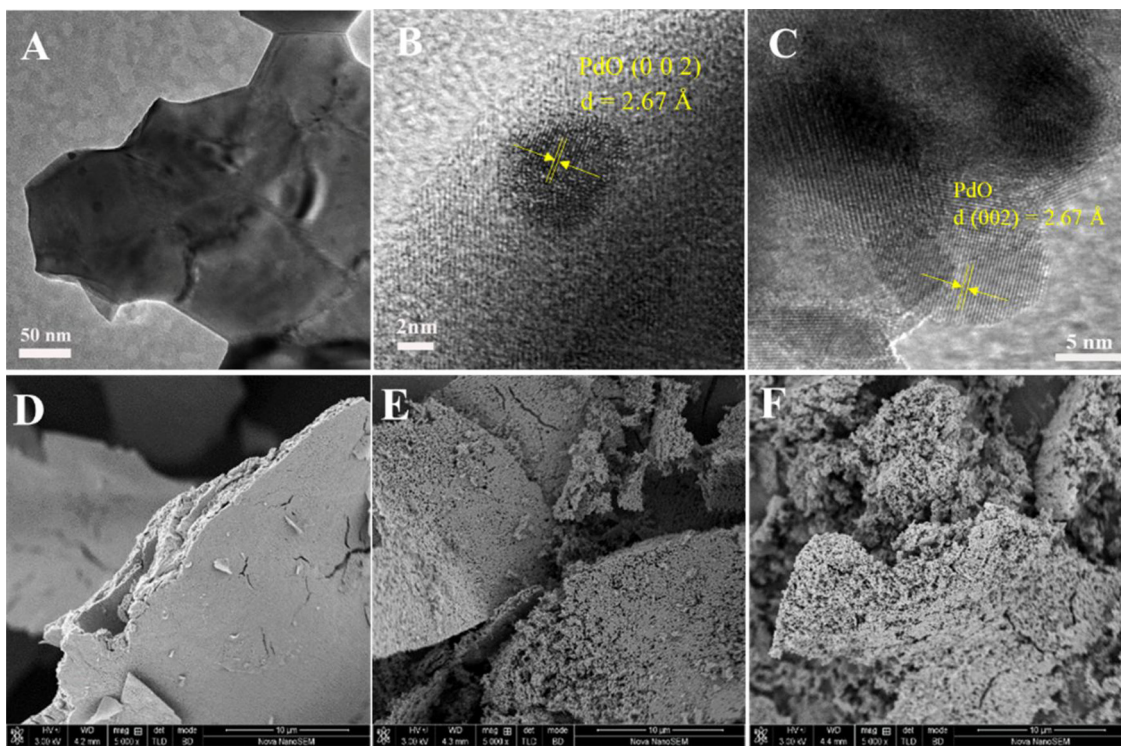


Fig. 3. HRTEM images (A–C) of the LAP-900 catalyst, and SEM images of the LAP-900 (D), LAP-H-30 (E) and LAP-H-90 (F) catalysts.

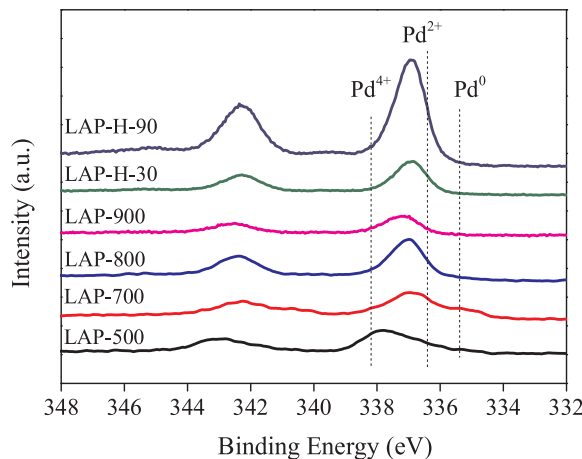


Fig. 4. Pd 3d XPS spectra of the LAP-500, LAP-700, LAP-800, LAP-900, LAP-H-30 and LAP-H-90 catalysts.

between Pd species and perovskite matrix. This indirectly proved that Pd species migrated from the bulk phase to the surface and subsurface of the catalyst. The surface element composition of the catalysts calcined at different temperatures was also listed in Table 1. It was predictable that the content of Pd on the surface of the catalyst increased with the increase in the calcination temperature of the catalyst, proving the presence of more Pd species on the surface and subsurface of the catalyst calcined at higher temperature.

XPS spectroscopy was also employed to determine the surface composition and the valence state of Pd on the surface of the LAP-H-30 and LAP-H-90 catalysts. It was noticeable that the surface element composition of the LAP-900 catalyst changed drastically after HNO₃ etching. As shown in Table 1, after acid treatment for 90 min, the atomic ratio of La to (La + Al + Pd) decreased from 39.1% to 28.4%, and the atomic ratio of Al to (La + Al + Pd) also decreased from 58.5% to 42.8%. In contrast, the atomic ratio of Pd to (La + Al + Pd)

significantly increased from 2.3% to 28.9%. These results indicated that a certain amount of La and Al on the surface of the LAP-900 catalyst was etched by the HNO₃, while the Pd species can be retained on the catalyst surface. The ICP results (shown in Table 1) also confirmed the increase in the Pd content of the catalysts after HNO₃ etching, *i.e.*, 4.2% over the LAP-900 catalyst vs. 8.9% over the LAP-H-90 catalyst. Additionally, compared to the LAP-900 catalyst, the Pd 3d_{5/2} peak for the LAP-H-30 and LAP-H-90 catalysts shifted to a lower binding energy (336.8 eV). Therefore, HNO₃ etching could not only modulate the surface composition but also the valence state of Pd. The Pd species in the LAP-900 catalyst were in the form of Pd⁸⁺ ($\delta > 2$), while a large amount of Pd species was exposed to the catalyst surface in the form of PdO after HNO₃ etching. As a result, the Pd 3d_{5/2} peak shifted to a lower binding energy for the LAP-H-30 and LAP-H-90 catalysts compared to the LAP-900 catalyst.

3.2. Redox property of the catalysts

3.2.1. H₂-TPR

Fig. 5A showed H₂-TPR profiles of the different catalysts. Only a weak reduction peak at 132 °C was observed below 400 °C for the LAP-500 and LAP-700 catalysts. Since the La³⁺ and Al³⁺ ions were very stable and hard to reduce below 300 °C, H₂ could only be consumed by the reduction of PdO_x species. Thus, it was revealed that most of the Pd species were distributed in the bulk phase of the LAP-500 and LAP-700 catalysts, leading to less chance to react with H₂. In contrast, a strong reduction peak at 68 °C appeared for the LAP-800 and LAP-900 catalysts, and it can be assigned to the reduction of Pd⁸⁺ ($\delta > 2$) → Pd⁰. Furthermore, the area of the reduction peak for the LAP-900 catalyst was higher than that for the LAP-800 catalyst. These results revealed that the increase in the calcination temperature of the catalyst can impel more Pd species to be present on the surface and subsurface of the catalyst, leading to the better redox property of the LAP-900 catalyst compared to the LAP-500, LAP-700 and LAP-800 catalysts.

As for the LAP-H-30 and LAP-H-90 catalysts, similar to the H₂-TPR profile of the LAP-900 catalyst, there was also a reduction peak at low

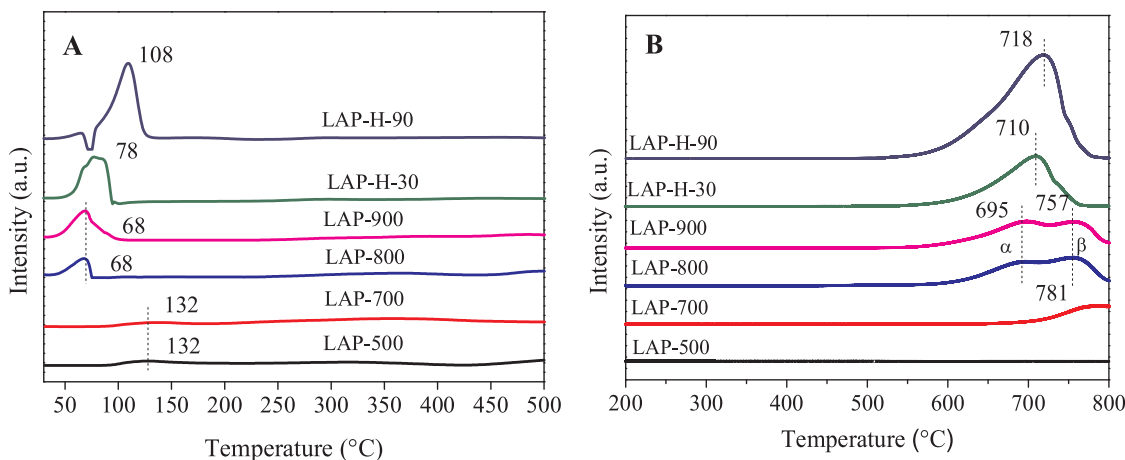
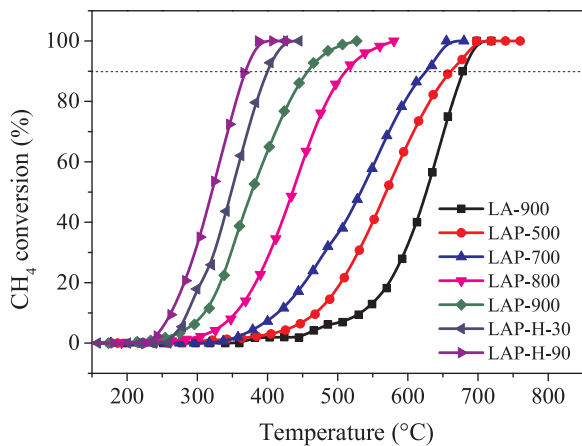
Fig. 5. H_2 -TPR (A) and O_2 -TPD profiles (B) of the different catalysts.

Fig. 6. The catalytic activity of the different catalysts for CH_4 combustion (Reaction conditions: 0.2 g catalyst; 1 vol. % CH_4 + 20 vol. % O_2 / N_2 balanced, total flow rate 50 mL/min and GHSV = 15 000 mL/ g·h).

temperature. In addition, a negative peak was observed for the LAP-H-90 catalyst, and it can be assigned to the decomposition of PdH_x . Compared to the LAP-900 catalyst, the area of the reduction peak for the LAP-H-30 and LAP-H-90 catalysts was increased obviously. Based on the characterization results, after HNO_3 etching, the Pd content in the catalyst increased and more Pd species were exposed on the surface and subsurface of the catalyst, which resulted in the increase in the H_2 consumption. On the other hand, the reduction peak for the LAP-H-30 and LAP-H-90 catalysts shifted to a high temperature compared to the LAP-900 catalyst, indicating that PdO_x species on the catalyst after HNO_3 etching were more difficult to reduce. In summary, the redox property ranked in the following order: LAP-H-90 > LAP-H-30 > LAP-900 catalysts.

3.2.2. O_2 -TPD

Fig. 5B showed the O_2 -TPD profiles of the different catalysts. No desorption peak was observed over the LAP-500 catalyst. In contrast, the LAP-700 catalyst exhibited one desorption peak at a temperature higher than 700 °C, while two overlapped desorption peaks (labelled as α and β) can be observed over the LAP-800 and LAP-900 catalysts. Furthermore, the ratio between the peak intensity of α and β peaks was higher over the LAP-900 catalyst than over the LAP-800 catalyst. It can be deduced that the α peak was assigned to the decomposition of PdO_x on the surface while the β peak was assigned to PdO_x species strongly bonded with La or Al existing on the subsurface of the catalyst [40,41]. This result demonstrated that the calcination of the catalyst at high

temperature would promote the migration of more PdO species from the bulk to the surface, consistent with the results of the structural characterizations. As a result, the catalysts calcined at the higher temperature can provide much more oxygen at > 550 °C.

Unlike the LAP-900 catalyst, only a strong desorption peak was observed over the LAP-H-30 and LAP-H-90 catalysts, assigned to the decomposition of PdO on the surface. After HNO_3 etching, many Pd species on the subsurface of the LAP-900 catalyst can be exposed to the catalyst surface, leading to the disappearance of the β peak assigned to Pd species located on the subsurface. However, the intensity of the α desorption peak for the LAP-H-30 and LAP-H-90 catalysts was higher than that for the LAP-900 catalyst, due to the more PdO species exposed on the surface of the catalyst after HNO_3 etching. Meanwhile, the desorption peak for the LAP-H-30 and LAP-H-90 catalysts shifted to a high temperature compared to the LAP-900 catalyst. This may be attributed to the strong interaction between the Pd species and perovskite matrix, consistent with the H_2 -TPR results.

3.3. Catalytic activity for CH_4 combustion

Based on the characterization of the structure and redox property of the catalysts prepared, the catalytic activity of the different catalysts for CH_4 combustion was tested finally. As shown in Fig. 6, LA-900 perovskite catalyst exhibited an extremely low catalytic activity for CH_4 combustion and the T_{90} (reaction temperature for 90% conversion of CH_4) was nearly up to 680 °C. However, the incorporation of Pd into the perovskite can significantly improve its catalytic activity for CH_4 combustion. Furthermore, with the increase in the calcination temperature of the catalyst, the catalytic activity of the catalysts prepared for CH_4 combustion increased. The corresponding TOF values of the catalysts with respect to Pd dispersion ranked in the order: 0.0466 s^{-1} (LAP-900) > 0.0282 s^{-1} (LAP-800) > 0.0155 s^{-1} (LAP-700) > 0.0071 s^{-1} (LAP-500), as shown in Table 1. As discussed in the previous section, the calcination of the catalyst at high temperature can expose a part of Pd species from the B sites of the perovskite lattice to the surface and subsurface of the catalyst, leading to the significant improvement of the catalytic activity of the catalyst for CH_4 combustion. On the other hand, as shown in Fig. 6, HNO_3 etching can further improve the catalytic activity of the LAP catalyst for CH_4 combustion. T_{90} for the LAP-H-30 and LAP-H-90 catalysts were 399 and 368 °C respectively, which were much lower than that of the LAP-900 catalyst (460 °C). Furthermore, the former two catalysts exhibited the higher TOF values than the LAP-900 catalyst, as shown in Table 1. To highlight the superior catalytic performance of the LAP-900 and LAP-H-90 catalysts for CH_4 combustion, their activities were compared with that of other reported catalysts based on TOF value, and the results are listed in Table S1. It was found that the catalytic activities of the LAP-900 and LAP-H-90

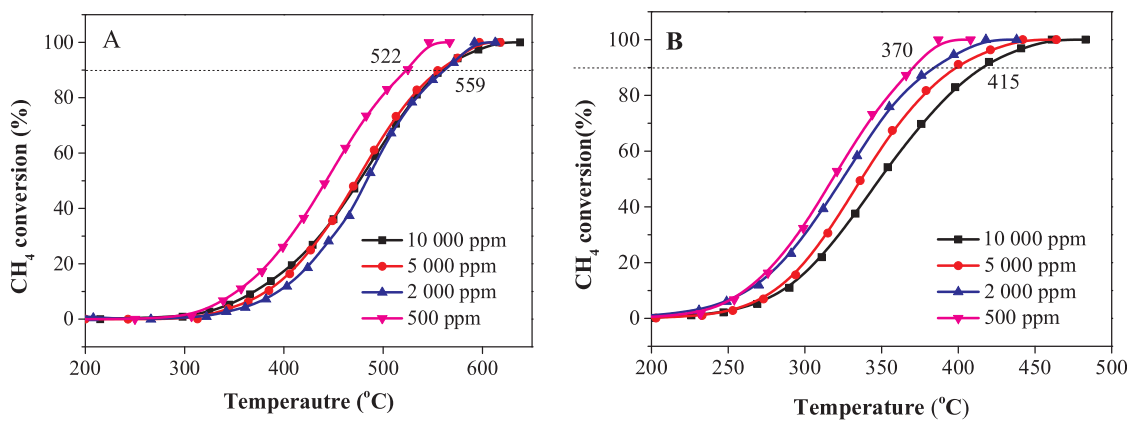


Fig. 7. The effect of CH_4 concentration on the catalytic activity of the LAP-900 (A) and LAP-H-90 (B) catalysts for CH_4 combustion (Reaction conditions: 0.2 g catalyst; 500–10000 ppm CH_4 , 20% O_2 , N_2 balance; GHSV = 100,000 mL/g·h).

catalysts were comparable to those of the high active Pd catalysts reported in the literatures without regard to the calcination temperature of the catalyst. However, the LAP-900 catalyst exhibited a superior catalytic activity compared to the catalyst calcined at high temperature (≥ 700 °C) in references, such as Pd/CeO_2 and $\text{PdPt}_{0.25}/\text{Al}_2\text{O}_3$ catalysts. These findings indicated that the LAP-900 and LAP-H-90 catalysts were the promising catalysts for the total oxidation of propane. Furthermore, the catalytic activities of $\text{LaAl}_{0.96}\text{Pd}_{0.04}\text{O}_3$ (2 wt.% Pd) and $\text{LaAl}_{0.98}\text{Pd}_{0.02}\text{O}_3$ (1 wt.% Pd) catalysts could also be improved by thermal treatment and acid etching, shown in Fig. S5, indicating that this method of active modulation had strong universality.

On this basis, in order to evaluate the catalytic performance of the catalysts more relevant to the theme of the applied catalysis, the catalytic activity of the LAP-900 and LAP-H-90 catalysts was further investigated under the different CH_4 feed gas composition and reactor space velocity. As shown in Fig. 7A, when the CH_4 concentration in feed gas increased from 500 to 2000 ppm, the CH_4 conversion at the same reaction temperature on the LAP-900 catalyst was slightly decreased, while it hardly changed when the CH_4 concentration further increased to 10,000 ppm. For the LAP-H-90 catalyst, the CH_4 conversion at the same reaction temperature slightly decreased with the increase in CH_4 concentration in feed gas from 500 to 10,000 ppm (Fig. 7B). Meanwhile, the catalytic activity of the LAP-900 and LAP-H-90 catalysts for CH_4 combustion under the space velocity of 15,000–200,000 mL/g·h was shown in Fig. 8. The catalytic activity of both the LAP-900 and LAP-H-90 catalysts gradually decreased with the increase in the space velocity from 15,000 to 200,000 mL/g·h, except the similar catalytic activity of the LAP-900 catalyst under the space velocity of 150000 and 200,000 mL/g·h. However, the degree of the catalytic activity decrease

was milder on the LAP-H-900 catalyst compared to the LAP-900 catalyst. Even under the space velocity of 200,000 mL/g·h, the LAP-H-90 catalyst still exhibited an excellent catalytic activity for CH_4 oxidation ($T_{90} = 441$ °C). These results demonstrated that the LAP-900 and LAP-H-90 catalysts had a strong adaptability to CH_4 concentration and the space velocity in CH_4 combustion.

The reaction stability of the LAP-900 and LAP-H-90 catalysts was also measured and the result was shown in Fig. 9A–C. The catalytic activity of both the LAP-900 and LAP-H-90 catalysts remain unchanged within 50 h at the temperature of 80% CH_4 conversion. Furthermore, the catalytic activity of the LAP-H-90 catalyst can be also retained completely after cycling four times. These results demonstrated the remarkable thermal stability of the LAP-900 and LAP-H-90 catalyst. Because of a large amount of Pd species located on the surface and subsurface of the LAP-900 catalyst originating from the migration of Pd species from the bulk phase, there was a strong interaction between Pd species and perovskite matrix. This specific structure of the LAP-900 catalyst can significantly promote the thermal stability of Pd species as active sites. As a result, the LAP-900 catalyst exhibited excellent reactive stability for CH_4 combustion. Similarly, HNO_3 etching mainly removed certain amounts of La and Al on the surface of the LAP-900 catalyst but did not reduce the interaction between Pd species and perovskite matrix. Therefore, the LAP-H-90 catalysts could maintain the high catalytic activity even after long time reaction and recycling four times.

On the other hand, as required for the practical use of the catalysts, water inevitably exist in the reaction gas, which might quickly poison the catalyst. Fig. 9D displayed the effect of H_2O on the activity of the LAP-900 and LAP-H-90 catalysts for CH_4 combustion. The catalyst was

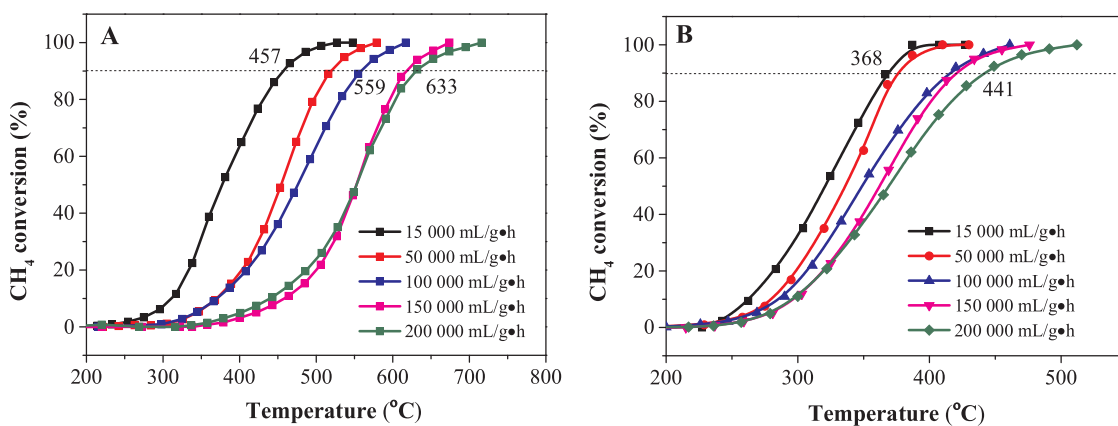


Fig. 8. The effect of space velocity on the catalytic activity of the LAP-900 (A) and LAP-H-90 (B) catalysts for CH_4 combustion (Reaction conditions: 0.2 g catalyst; 1% CH_4 , 20% O_2 , N_2 balance; GHSV = 15,000–200,000 mL/g·h).

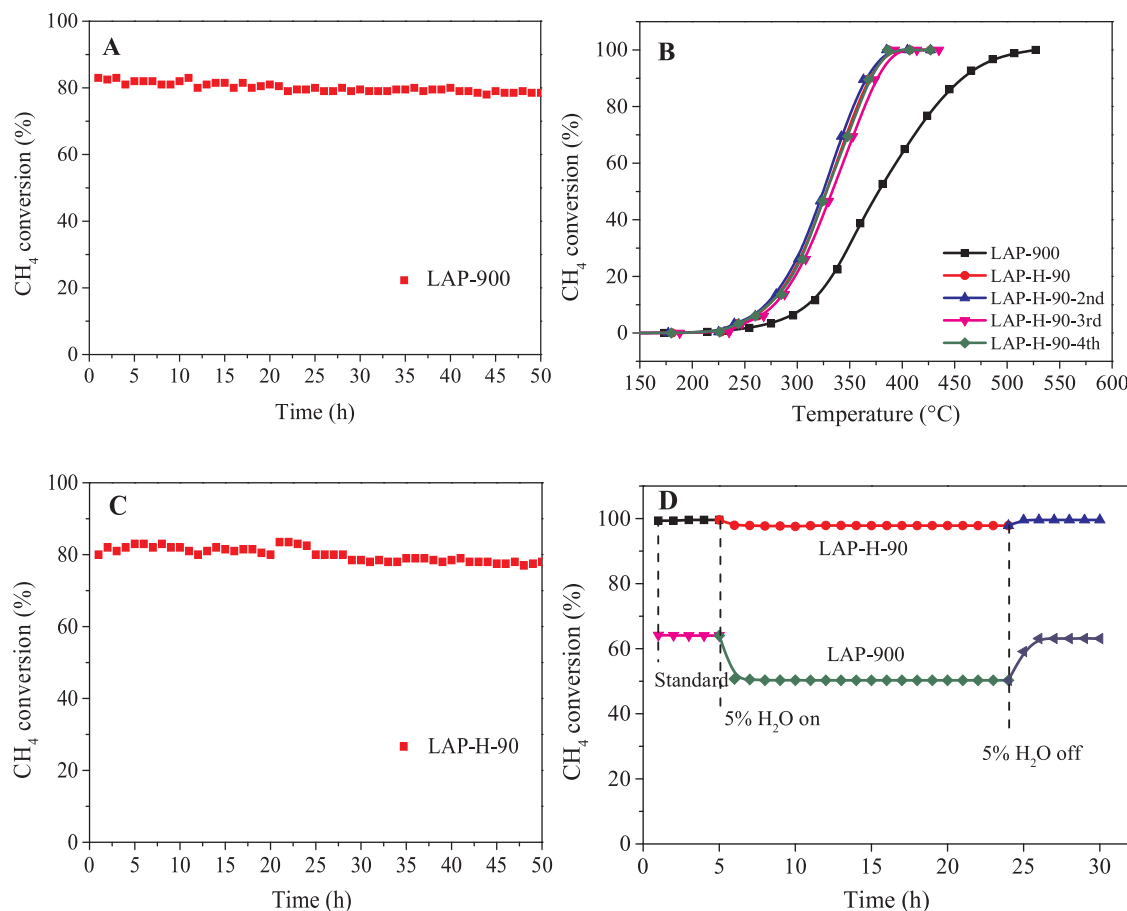


Fig. 9. The reaction stability of LAP-900 at 430 °C (A), recycling experiments of the LAP-H-90 catalyst for CH₄ combustion (B), the reaction stability of the LAP-H-90 catalyst at 350 °C (C), and effect of water on the catalytic activities of the LAP-H-30 and LAP-900 catalysts for CH₄ combustion (D) (Reaction conditions: 0.2 g sample; 400 °C; 1 vol. % CH₄ + 20 vol. % O₂ + 5 vol. % H₂O (when used) /N₂ balanced, total flow rate 50 mL/min and GHSV = 15,000 mL/g·h).

kept under the reaction conditions for 4 h (T = 400 °C) and then 5 vol. % H₂O was introduced into the feed gas mixture for 20 h. After that, the reaction gas atmosphere was recovered to the initial conditions for 7 h. The results showed that when 5 vol. % H₂O was introduced into the feed gas, CH₄ conversion slightly decreased from 99.7% to 97.8% over the LAP-H-90 catalyst, while from 64.2% to 50.3% over the LAP-900 catalyst, indicating a high water resistance performance of the LAP-900 and LAP-H-90 catalysts. Furthermore, it was interesting that the catalytic activities of both the catalysts can be completely recovered within 1 h after removing the H₂O from the feed gas, confirming the excellent water resistance of the LAP-H-30 and LAP-900 catalysts.

3.4. Discussion

In general, perovskite oxides exhibit the low catalytic performances in deep oxidation reactions in waste gas pollution control. One of the most effective strategies to improve its catalytic performance is the substitution of B cations in perovskite oxides with noble metal elements. However, the incorporation of noble metal into the perovskite would reduce the utilization of noble metal, because most of the noble metal in the B sites of the perovskite lattice cannot participate in the catalytic reaction. In contrary, when noble metal was supported on perovskite oxide, the thermal stability of noble metal particle was unsatisfactory in general, which negated its advantage in the utilization of noble metal. Therefore, a new and simple method was desperately needed to construct the noble metal in perovskite matrix and as close as possible to the surface and subsurface of perovskite oxide.

Herein, a new path to tune the distribution of noble metal on the perovskite oxide by synergistic effect of thermal treatment and acid

etching was proposed. LaAl_{0.9}Pd_{0.1}O₃ perovskite catalyst prepared by the citric acid sol-gel method were used as a model. First of all, the obtained perovskite precursor was calcined at different temperature, such as 500, 700, 800 and 900 °C. XRD and Raman results indicated that when calcined at 500 and 700 °C, the catalysts exhibited amorphous structure and Pd species were highly distributed in the bulk phase. With the increase in the calcination temperature up to 800 and 900 °C, the perovskite structure formed and Pd species were inclined to migrate to the perovskite surface, leading to more PdO species present on the surface and subsurface of the LAP-800 and LAP-900 catalysts compared to the LAP-500 and LAP-700 catalysts. TEM and CO-pulse experiment further confirmed the presence of more PdO species on the surface and subsurface of the LAP-900 catalyst. XPS results indicated that Pd species for all of the catalysts were in the form of Pd⁸⁺ ($\delta > 2$). However, the shift of Pd binding energy and the change in the surface element composition of the catalysts revealed that the Pd content on the catalyst surface increased with the increase in the calcination temperature of the catalyst, accompanied by the reduction in the interaction between Pd species and perovskite matrix. All these characterization results demonstrated the migration of Pd species during the calcination at high temperature and more Pd species present on the surface and subsurface of the catalysts calcined at high temperature.

Based on the migration of Pd species, the catalysts calcined at high temperature exhibited the high redox property and can provide more oxygen, shown in H₂-TPR and O₂-TPD results. As a result, the catalytic activity of the catalysts prepared for CH₄ combustion increased with the increase in the calcination temperature. The corresponding TOF values of the catalysts with respect to Pd dispersion ranked in the order: 0.0466 s⁻¹ (LAP-900) > 0.0282 s⁻¹ (LAP-800) > 0.0155 s⁻¹ (LAP-

700) > 0.0071 s⁻¹ (LAP-500). Furthermore, the LAP-900 catalyst had a strong adaptability to CH₄ concentration (500~10 000 ppm) and the space velocity (15 000~200 000 mL/g·h) in CH₄ combustion. Meanwhile, the catalytic activity of the LAP-900 catalyst remained unchanged within 50 h at the temperature of 80% CH₄ conversion. As a large amount of Pd species located on the surface and subsurface of the LAP-900 catalyst originated from the migration of Pd species from the bulk phase, there was a strong interaction between Pd species and perovskite matrix, leading to the excellent reactive stability of the LAP-900 catalyst for CH₄ combustion.

Although the catalytic activity of the catalyst calcined at high temperature for CH₄ combustion was significantly improved, there was still a large amount of Pd occupying the B site existing in the bulk phase and subsurface layer. These Pd species would have less chance to participate in the catalytic reaction. Therefore, the LAP-900 catalyst was etched with a certain concentration of HNO₃ for 30 min and 90 min respectively, to further tuning the distribution of Pd species on the LAP-900 catalyst. XRD and SEM results revealed that although the smooth surface morphology of the LAP-900 catalyst was destructed after HNO₃ etching, the LAP-900 catalyst maintained the perovskite structure and its crystallite degree decreased slightly. Besides, a certain amount of agglomerated PdO species appeared on the surface of the LAP-H-90 catalyst. XPS and ICP results showed that a certain amount of La and Al on the surface of the LAP-900 catalyst was etched by the HNO₃ reliably, leading to more Pd species being exposed on the surface of the LAP-900 catalyst. Based on the surface structure tuning, the LAP-H-30 and LAP-H-90 catalysts exhibited the higher catalytic activity for CH₄ combustion than that of the LAP-900 catalyst. The TOF values of the LAP-H-30 and LAP-H-90 catalysts with respect to Pd dispersion increased to 0.0963 and 0.1183 s⁻¹ respectively, compared to 0.0466 s⁻¹ of the LAP-900 catalyst. Furthermore, the strong adaptability to CH₄ concentration and the space velocity of the LAP-900 catalyst can be maintained after HNO₃ etching. On the other hand, LAP-H-90 catalysts also exhibited the high reaction stability for CH₄ combustion. More broadly, the water resistance of the LAP-900 catalyst can be also improved after HNO₃ etching. As discussed in characterization results, HNO₃ etching mainly removed certain amounts of La and Al on the surface of the LAP-900 catalyst but did not reduce the interaction between Pd species and perovskite matrix. Therefore, the LAP-H-90 catalysts could maintain the high stability even after long time reaction and recycling four times.

4. Conclusions

LaAl_{0.9}Pd_{0.1}O₃ perovskite catalyst was prepared by the citric acid sol-gel method and calcined at different temperatures. The LaAl_{0.9}Pd_{0.1}O₃ catalyst was in the form of an amorphous structure after calcining at a low temperature (500 °C and 700 °C), and the Pd species were highly distributed in the bulk phase. These catalysts showed a low redox property and catalytic activity for CH₄ combustion. However, after the LaAl_{0.9}Pd_{0.1}O₃ catalyst was calcined at 800 °C and 900 °C, the perovskite structure formed, and part of the Pd species exsolved from the bulk to the surface and subsurface of the catalyst. Consequently, the redox property of the catalyst was significantly prompted, leading to the obvious improvement of the catalytic activity of the catalyst for CH₄ combustion. On this basis, the surface composition of the LAP-900 catalyst was further modulated with HNO₃ etching. After acid treatment, a larger amount of Pd species was exposed on the surface. As a result, the LAP-H-30 and LAP-H-90 catalysts showed a higher catalytic activity and stability for CH₄ oxidation compared to the LAP-900 catalyst. In summary, thermal treatment and HNO₃ etching would provide a facile and simple strategy to modulate the surface composition of noble metal doped perovskite oxide, subsequently improving the catalytic activity of the perovskite catalysts. This new path based on the synergistic effect of thermal treatment and acid etching will open a window for us to prepare perovskite catalysts with excellent catalytic

performance for oxidation reactions by tuning the surface composition.

Acknowledgments

This work was financially supported by the National Key Research and Development Program of China (2016YFC0204300), the National Natural Science Foundation of China (21577034), Science and Technology Commission of Shanghai Municipality (16ZR1407900) and Fundamental Research Funds for the Central Universities (222201717003).

Appendix A. Supplementary data

Supplementary material related to this article can be found, in the online version, at doi:<https://doi.org/10.1016/j.apcatb.2018.08.038>.

References

- [1] G. Zhu, J. Han, D.Y. Zemlyanov, F.H. Ribeiro, *J. Am. Chem. Soc.* 126 (2004) 9896–9897.
- [2] W.C. Zhan, Q. He, X.F. Liu, Y. Guo, Y. Wang, L. Wang, Y. Guo, A.Y. Borisevich, J. Zhang, G. Lu, *J. Am. Chem. Soc.* 138 (49) (2016) 16130–16139.
- [3] Z. Hu, S. Qiu, Y. You, Y. Guo, Y.L. Guo, L. Wang, W.C. Zhan, G.Z. Lu, *Appl. Catal. B* 225 (2018) 110–120.
- [4] Q. Dai, S. Bai, Y. Lou, X. Wang, Y. Guo, G. Lu, *Nanoscale* 8 (2016) 9621–9628.
- [5] Y. Lou, P. He, L. Zhao, H. Song, *Fuel* 183 (2016) 396–404.
- [6] Y.H. Chin, C. Buda, M. Neurock, E. Iglesia, *J. Am. Chem. Soc.* 135 (2013) 15425–15442.
- [7] J. Nilsson, P.-A. Carlsson, S. Fouladvand, N.M. Martin, J. Gustafson, M.A. Newton, E. Lundgren, H. Grönbeck, M. Skoglundh, *ACS Catal.* 5 (2015) 2481–2489.
- [8] C.K. Shi, L.F. Yang, J.X. Cai, *Fuel* 86 (2007) 106–112.
- [9] T.W. Hansen, A.T. DeLaRiva, S.R. Challa, A.K. Datye, *Acc. Chem. Res.* 46 (2013) 1720–1730.
- [10] G. Prieto, J. Zečević, H. Friedrich, K.P. de Jong, P.E. de Jongh, *Nat. Mater.* 12 (2013) 34–39.
- [11] N. Masoud, L. Delannoy, H. Schaink, A. van der Eerden, J.W. de Rijk, T.A.G. Silva, D. Banerjee, J.D. Meeldijk, K.P. de Jong, C. Louis, P.E. de Jongh, *ACS Catal.* 7 (2017) 5594–5603.
- [12] S. Tomiyama, R. Takahashi, S. Sato, T. Sodesawa, S. Yoshida, *Appl. Catal. A Gen.* 241 (2003) 349–361.
- [13] R. Di Monte, P. Fornasiero, J. Kašpar, P. Rumori, G. Gubitosa, M. Graziani, *Appl. Catal. B* 24 (2000) 157–167.
- [14] V. Fung, F. P-Garzon, Z.L. Wu, D. Jiang, *Catal. Sci. Technol.* 8 (2018) 702–709, <https://doi.org/10.1039/C7CY01791J>.
- [15] Z.Y. Zhao, L. Wang, J. Ma, Y.F. Feng, X.M. Cao, W.C. Zhan, Y.L. Guo, Y. Guo, G.Z. Lu, *RSC Adv.* 7 (2017) 15211–15221.
- [16] C.C. Tian, X. Zhu, C.W. Abney, X.F. Liu, G.S. Foo, Z.L. Wu, M.J. Li, H.M. Meyer, S. Brown, S.M. Mahurin, S.J. Wu, S.Z. Yang, J.Y. Liu, S. Dai, *ACS Catal.* 7 (2017) 3388–3393.
- [17] D.Y. Yoon, Y.J. Kim, J.H. Lim, B.K. Cho, S.B. Hong, I.S. Nam, J.W. Choung, *J. Catal.* 330 (2015) 71–83.
- [18] W.C. Zhan, S.Z. Yang, P.F. Zhang, Y.L. Guo, G.Z. Lu, M.F. Chisholm, S. Dai, *Chem. Mater.* 29 (2017) 7323–7329.
- [19] C.H. Zhang, C. Wang, S. Gil, A. Boreave, L. Retailleau, Y.L. Guo, J.L. Valverdec, A. Giroir-Fendler, *Appl. Catal. B* 201 (2017) 552–560.
- [20] Q.J. Meng, W.L. Wang, X.L. Weng, Y. Liu, H.Q. Wang, Z.B. Wu, *J. Phys. Chem. C* 120 (2016) 3259–3266.
- [21] F. Teng, W. Han, S.H. Liang, B. Gaugeu, R.L. Zong, Y.F. Zhu, *J. Catal.* 250 (2007) 1–11.
- [22] H.Y. Zhu, P.F. Zhang, S. Dai, *ACS Catal.* 5 (2015) 6370–6385.
- [23] S. Royer, D. Duprez, F. Can, X. Courtois, C. Batiot-Dupeyrat, S. Laassiri, H. Almandari, *Chem. Rev.* 114 (2014) 10292–10368.
- [24] D. Neagu, G. Tsekouras, D.N. Miller, H. Ménard, J.T.S. Irvine, *Nat. Chem.* 5 (2013) 916–923.
- [25] H. Dulli, P.A. Dowben, S.-H. Liou, E.W. Plummer, *Phys. Rev. B, Matter Mater. Phys.* 62 (2000) 629–632.
- [26] Z. Cai, Y. Kuru, J.W. Han, Y. Chen, B. Yıldız, *J. Am. Chem. Soc.* 133 (2011) 17696–17704.
- [27] A.Y. Yan, V. Maragou, A. Arico, M.J. Cheng, P. Tsakarlas, *Appl. Catal. B* 76 (2007) 320–327.
- [28] C.H. Zhang, W.C. Hua, C. Wang, Y.L. Guo, Y. Guo, G.Z. Lu, A. Baylet, A. Giroir-Fendler, *Appl. Catal. B* 134–135 (2013) 310–315.
- [29] C.H. Zhang, C. Wang, W.C. Zhan, Y.L. Guo, Y. Guo, G.Z. Lu, A. Baylet, A. Giroir-Fendler, *Appl. Catal. B* 129 (2013) 509–516.
- [30] D.Y. Yoon, E. Lim, Y.J. Kim, B.K. Cho, I.S. Nam, J.W. Choung, S.B. Yoo, *ACS Comb. Sci.* 16 (2014) 614–623.
- [31] D.Y. Yoon, E. Lim, Y.J. Kim, J.H. Kim, T. Ryu, S. Lee, B.K. Cho, I.S. Nam, J.W. Choung, S.B. Yoo, *J. Catal.* 319 (2014) 182–193.
- [32] G. Bulgan, F. Teng, S.H. Liang, W.Q. Yao, Y.F. Zhu, *Acta Phys. Sin.* 23 (2007) 1387–1392.

[33] C.H. Zhang, Y.L. Guo, Y. Guo, G.Z. Lu, A. Boreave, L. Retailleau, A. Baylet, A. Giroir-Fendler, *Appl. Catal. B* 148-149 (2014) 490–498.

[34] A. Giroir-Fendler, M. Alves-Fortunato, M. Richard, C. Wang, J.A. Díaz, S. Gil, C.H. Zhang, F. Can, N. Bion, Y.L. Guo, *Appl. Catal. B* 180 (2016) 29–37.

[35] S.H. Liang, T.G. Xu, F. Teng, R.L. Zong, Y.F. Zhu, *Appl. Catal. B* 96 (2010) 267–275.

[36] A. Musialik-Piotrowska, H. Landmesser, *Catal. Today* 137 (2008) 357–361.

[37] U.G. Singh, J. Li, J.W. Bennett, A.M. Rappe, R. Seshadri, S.L. Scott, *J. Catal.* 249 (2007) 349–358.

[38] H. Ziae-Azad, A. Khodadadi, P. Esmailnejad-Ahranjani, Y. Mortazavi, *Appl. Catal. B* 102 (2011) 62–70.

[39] W.C. Zhan, Y. Shu, Y.J. Sheng, H.Y. Zhu, Y.L. Guo, L. Wang, Y. Guo, J.S. Zhang, G.Z. Lu, S. Dai, *Angew. Chem. Int. Ed.* 56 (2017) 4494–4498.

[40] Y. Nishihata, J. Mizuki, T. Akao, H. Tanaka, M. Uenishi, M. Kimura, T. Okamoto, N. Hamada, *Nature* 418 (2002) 164–167.

[41] M.B. Katz, G.W. Graham, Y. Duan, H. Liu, C. Adamo, D.G. Schlam, X. Pan, *J. Am. Chem. Soc.* 133 (2011) 18090–18093.

[42] H. Tanaka, M. Taniguchi, M. Uenishi, N. Kajita, I. Tan, Y. Nishihata, J. Mizuki, K. Narita, M. Kimura, K. Kaneko, *Angew. Chem. Int. Ed.* 45 (2006) 5998–6002.

[43] Z.X. Tian, A. Uozumi, I. Hamada, S. Yanagisawa, H. Kizaki, K. Inagaki, Y. Morikawa, *Nanoscale Res. Lett.* 8 (2013) 203–209.

[44] Z.X. Tian, K. Inagaki, Y. Morikawa, *Curr. Appl. Phys.* 12 (2012) S105–S109.

[45] W.Z. Si, Y. Wang, S. Zhao, F. Hu, J.H. Li, *Environ. Sci. Technol.* 50 (2016) 4572–4578.

[46] W.Z. Si, Y. Wang, Y. Peng, J.H. Li, *Angew. Chem.* 127 (2015) 8065–8068.

[47] K.K. Huang, X.F. Chu, L. Yuan, W.C. Feng, X.F. Wu, X.Y. Wang, S.H. Feng, *Chem. Commun.* 50 (2014) 9200–9203.

[48] Y.J. Luo, K.C. Wang, J.C. Zuo, Q.G. Qian, Y.X. Xu, X.P. Liu, H. Xue, Q.H. Chen, *Catal. Sci. Technol.* 7 (2017) 496–501.

[49] Y. Peng, W.Z. Si, J.M. Luo, W.K. Su, H.Z. Chang, J.H. Li, J.M. Hao, J. Crittenden, *Environ. Sci. Technol.* 50 (2016) 6442–6448.

[50] M.T. Klug, A. Oshero, A.A. Haghigirad, S.D. Stranks, P.R. Brown, S. Bai, J.T.-W. Wang, X.N. Dang, V. Bulović, H.J. Snaith, A.M. Belcher, *Energy Environ. Sci.* 10 (2017) 236–246.

[51] J.N. Hui, D. Neagu, D.N. Miller, X.L. Yue, C.S. Ni, J.T.S. Irvine, *Solid State Ion.* 315 (2018) 126–130.

[52] D.D. He, G.H. He, H.Q. Jiang, Z.K. Chen, M.H. Huang, *Chem. Commun.* 53 (2017) 5132–5135.

[53] Y.R. Wang, Z.B. Yang, F.L. Lu, C. Jin, J. Wu, M. Shen, R.Z. Yang, F.L. Chen, *RSC Adv.* 5 (2015) 974–980.

[54] Y.D. Cao, R. Ran, X.D. Wu, B.H. Zhao, J. Wan, D. Weng, *Appl. Catal. A Gen.* 457 (2013) 52–61.

[55] A. Fyssler, A. Winkler, O. Safonova, M. Nachtegaal, S.K. Matam, P. Hug, A. Weidenkaff, D. Ferri, *Chem. Mater.* 24 (2012) 1864–1875.

[56] A. Fyssler, P. Mandaliev, A. Winkler, P. Hug, O. Safonova, R. Figi, A. Weidenkaff, D. Ferri, *J. Phys. Chem. C* 114 (2010) 4584–4594.

[57] H.Y. Tan, J. Wang, S.Z. Yu, K.B. Zhou, *Environ. Sci. Technol.* 49 (2015) 8675–8682.

[58] E.M. Slavinskaya, R.V. Gulyaev, A.V. Zadesenets, O.A. Stonkus, V.I. Zaikovskii, Yu.V. Shubin, S.V. Korenev, A.I. Boronin, *Appl. Catal. B* 91–103 (2015) 166–167.

[59] R.V. Gulyaev, A.I. Stadnichenko, E.M. Slavinskaya, A.S. Ivanova, S.V. Koscheev, A.I. Boronin, *Appl. Catal. A Gen.* 439–440 (2012) 41–50.